THE JOURNAL OF BIOLOGICAL CHEMISTRY VOL. 286, NO. 39, pp. 34311–34324, September 30, 2011


# The Rho1 GTPase-activating Protein CgBem2 Is Required for Survival of Azole Stress in *Candida glabrata*[*] [S]

Received for publication, May 25, 2011, and in revised form, July 19, 2011 Published, JBC Papers in Press, August 8, 2011, DOI 10.1074/jbc.M111.264671

**Sapan Borah**[1], **Raju Shivarathri, and Rupinder Kaur**[2]

*From the Centre for DNA Fingerprinting and Diagnostics, Building 7, Gruhakalpa, 5-4-399/B, Nampally, Hyderabad 500001, India*

**Invasive fungal infections are common clinical complications of neonates, critically ill, and immunocompromised patients worldwide. *Candida* species are the leading cause of disseminated fungal infections, with *Candida albicans* being the most prevalent species. *Candida glabrata*, the second/third most common cause of candidemia, shows reduced susceptibility to a widely used antifungal drug fluconazole. Here, we present findings from a screen of 9134 *C. glabrata* Tn*7* insertion mutants for altered survival profiles in the presence of fluconazole. We have identified two components of RNA polymerase II mediator complex, three players of Rho GTPase-mediated signaling cascade, and two proteins implicated in actin cytoskeleton biogenesis and ergosterol biosynthesis that are required to sustain viability during fluconazole stress. We show that exposure to fluconazole leads to activation of the protein kinase C (PKC)-mediated cell wall integrity pathway in *C. glabrata*. Our data demonstrate that disruption of a RhoGAP (GTPase activating protein) domain-containing protein, CgBem2, results in bud-emergence defects, azole susceptibility, and constitutive activation of CgRho1-regulated CgPkc1 signaling cascade and cell wall-related phenotypes. The viability loss of *Cgbem2*Δ mutant upon fluconazole treatment could be partially rescued by the PKC inhibitor staurosporine. Additionally, we present evidence that *CgBEM2* is required for the transcriptional activation of genes encoding multidrug efflux pumps in response to fluconazole exposure. Last, we report that Hsp90 inhibitor geldanamycin renders fluconazole a fungicidal drug in *C. glabrata*.**

Hospital-acquired fungal infections pose a major health and economic challenge. *Candida* species are the leading cause of disseminated fungal infections and rank fourth among the most common nosocomial blood culture isolates in intensive care units (1, 2). Although *Candida albicans* still accounts for about 60% of total blood stream infections, systemic infections due to non-*albicans* species of *Candida* such as *Candida glabrata*, *krusei*, *tropicalis*, and *parapsilosis* have increased significantly in the last two decades (2, 3). *C. glabrata* is the second or third most common yeast pathogen found in blood stream infections depending upon the geographical location (3). The recent emergence of *C. glabrata* as a major nosocomial threat has been associated with its reduced susceptibility to azole antifungal agents (3, 4).

Fluconazole is a widely employed antifungal drug due to its efficacy, low toxicity, oral availability, well tolerability, and cost-effectiveness (5). Fluconazole belongs to the triazole class of antifungals and acts by inhibiting the cytochrome P450-dependent enzyme lanosterol 14α-demethylase, Erg11, an essential enzyme of the ergosterol biosynthesis pathway (6). Erg11 converts lanosterol to ergosterol, an important component of the fungal cell membrane. Inhibition of Erg11 results in the depletion of ergosterol from the plasma membrane and accumulation of 14 α-methylated sterol intermediates, ultimately causing growth arrest (6). *C. glabrata* shows low inherent susceptibility to fluconazole and a global trend in emergence of fluconazole resistant strains of *C. glabrata* has been observed (3, 4).

In addition to the reduced susceptibility to this fungistatic drug, *C. glabrata* can acquire further resistance to fluconazole by several mechanisms such as loss of mitochondrial function, alteration/overexpression of the target enzyme (CgErg11), and increased efflux due to the overexpression of ABC (ATP binding cassette) class of multidrug efflux transporters (CgCdr1, CgCdr2, and CgSnq2) (7–11). *CgCDR1*, *CgCDR2*, and *CgSNQ2* are under the transcriptional regulation of a $Zn_2Cys_6$ zinc cluster-containing transcription factor, CgPdr1 (12, 13). CgPdr1 can directly bind to drugs and xenobiotics and stimulates drug efflux (14). Mutations in CgPdr1 rendering it hyperactive contribute to fluconazole resistance in clinical isolates (12, 15).

Stress response signaling pathways have been shown to modulate azole susceptibility in fungal pathogens (16, 17). Inhibition of calcineurin-mediated calcium signaling augments the effect of azoles and makes them fungicidal in *Saccharomyces cerevisiae*, *C. albicans*, *C. glabrata*, and *C. krusei* (10, 18, 19). Additionally, *C. albicans* and *S. cerevisiae* mutants disrupted for genes involved in cyclic AMP/protein kinase A signaling pathway are hypersusceptible to fluconazole (20). Furthermore, genetic or chemical abrogation of function of a highly conserved chaperone Hsp90 leads to antifungal drug susceptibility in diverse fungi (21).

An essential role for Hsp90, calcineurin, and protein kinase C (PKC) in tolerance to the ergosterol biosynthesis inhibitor class of drugs has recently been reported for *S. cerevisiae* and *C. albicans* (22). The Pkc1 serine/threonine kinase in *S. cerevisiae* is essential for growth and regulates a highly conserved cell wall

[*] This work was supported in part by Innovative Young Biotechnologist Award BT/BI/12/040/2005 from the Department of Biotechnology, Government of India and by core funds of Centre for DNA Fingerprinting and Diagnostics, Hyderabad, India.

[S] The on-line version of this article (available at http://www.jbc.org) contains supplemental Tables S1–S3 and Figs. S1–S6.

[1] Recipient of a Senior Research Fellowship from Department of Biotechnology, Government of India.

[2] To whom correspondence should be addressed. Tel.: 91-40-24749408; Fax: 91-40-24749448; E-mail: rkaur@cdfd.org.in.

integrity (CWI)[3] pathway, composed of a linear array of mitogen-activated protein kinases (MAPKs), Pkc1-Bck1-Mkk1/Mkk2-Slt2 (23). Slt2 is the terminal serine/threonine MAPK and culminates the response of the PKC cascade to environmental stress signals through activation of the transcription factors Swi4/Swi6 and Rlm1 (23, 24).

An upstream component of Pkc1-activated MAPK cascade in *S. cerevisiae* is Rho1, a small guanosine triphosphatase (GTPase) that is positively and negatively regulated by GDP-GTP exchange factors (GEFs) and GTPase-activating proteins (GAPs) and GDP dissociation inhibitors, respectively (25, 26). Rho1 is active in the GTP-bound form; Rho1-GAPs increase the GTPase activity of Rho1 via a highly conserved, ~180-residue GAP domain and convert Rho1-GTP to inactive Rho1-GDP form, thus acting as negative regulators of the Rho1-PKC cascade (26). Rho1 acts as a multifunctional regulator through several distinct effector proteins including 1,3-$\beta$-D-glucan synthase (Fks1/Fks2), Pkc1, formin (Bni1), and the transcription factor Skn7 (26). The Rho1-PKC cascade plays an important role in cell wall biosynthesis, actin organization, morphogenesis, and survival during environmental stresses (22, 27, 28).

Although low inherent susceptibility/high intrinsic resistance of *C. glabrata* to the azole class of drugs including fluconazole has been well documented for the past two decades, the genetic and molecular basis of this resistance remains poorly understood. In this regard we had previously screened 9216 random Tn*7* insertion mutants for altered fluconazole susceptibility profiles and had identified a total of 10 and 17 mutants conferring fluconazole resistance and fluconazole sensitivity, respectively (10). Here we present findings from a screen of a non-overlapping set of 9134 mutants encompassing about ¼ of the *C. glabrata* genome for the inability to survive fluconazole stress. We report that mutants disrupted for components of RNA polymerase II mediator complex, PKC-mediated CWI pathway, and actin cytoskeleton biogenesis machinery are unable to retain viability during fluconazole treatment. Our data demonstrate that deletion of the Rho1 GTPase-activating protein (RhoGAP) CgBem2 results in azole susceptibility and constitutive activation of CgRho1 GTPase and of terminal MAPK CgSlt2. Furthermore, we show that inhibition of PKC signaling by staurosporine could partially rescue the fluconazole-induced viability loss of *Cgbem2*Δ cells. In addition, our data suggest that CgBem2 is required for the activation of multidrug transporters upon fluconazole exposure.

## EXPERIMENTAL PROCEDURES

*Strains and Culture Conditions—C. glabrata* wild-type and mutant strains were grown either in rich medium (YPD; 1% yeast extract, 2% peptone, and 2% dextrose), CAA medium (0.67% yeast nitrogen base without amino acids, 0.6% casamino acids, and 2% dextrose), or in synthetically defined yeast nitrogen base (0.67% yeast nitrogen base and 2% dextrose) medium at 30 °C with shaking at 200 rpm. Bacterial strains were grown at 37 °C in LB medium containing 30 $\mu$g/ml kanamycin or 60 $\mu$g/ml ampicillin. 2% agar was added to the plates. Logarithmic phase cells were obtained by growing overnight cultures in fresh yeast nitrogen base/YPD/CAA medium for 4 h at 30 °C. The strains, plasmids, and primers used are listed in supplemental Tables 1 and 2.

*Screening of Mutant Library*—Mutants were grown in YPD medium in 96-well plates overnight at 30 °C. Cell cultures were diluted 150-fold in PBS, and 5 $\mu$l of the diluted culture was spotted onto YPD plates containing different concentrations of fluconazole or methylene blue or in combination using a 96-pin replicator. Plates were incubated at 30 °C, growth profiles were scored after 24–48 h, and mutants were selected. Integration of Tn*7* insertion in the mutant genome via homologous recombination was confirmed by PCR as described previously (29).

*Knock-out Generation—C. glabrata* ORFs were disrupted by homologous recombination with a cassette-containing *nat1* gene, coding for nourseothricin acetyltransferase (imparts resistance to nourseothricin) flanked by 5′- and 3′-UTR regions of the gene. The 5′- and 3′-UTR (nearly 500 bp) of the genes were amplified from wild-type genomic DNA. Both the 5′ and 3′-UTR were fused to one-half each of the *nat1* gene amplified from a plasmid. The two *nat1*-amplified fragments share an ~300–350-bp complimentary region. The fused PCR products were co-transformed into the wild-type strain, and the transformants were plated on YPD. After incubation at 30 °C for 12–16 h to allow homologous recombination within the *nat1* fragments and with the genomic loci, cells were replica-plated onto a YPD plate supplemented with 200 $\mu$g/ml nourseothricin and further incubated for 24 h. Nourseothricin-resistant colonies were purified and checked for gene disruption via homologous recombination by PCR.

*Cloning of CgORFs—CgBEM2* (6.36 kb), *CgSLT2* (1.47 kb), and *CgRHO1* (0.63 kb) ORFs were PCR-amplified from genomic DNA of the wild-type strain using high fidelity Platinum Pfx DNA polymerase with primers carrying restriction sites for SmaI and SalI. Amplified fragments were cloned downstream of the *PGK1* promoter into the SmaI-SalI sites present in the pGRB2.2 plasmid. Clones were verified by PCR, sequencing, and complementation analysis.

*Site-directed Mutagenesis*—The arginine residue (AGA codon) at the 1957 amino acid position of CgBem2 was replaced with an alanine residue (GCA codon) using mutagenic primers. For this, the C-terminal sequence of *CgBEM2* (4671–6360) was excised out (SphI-SalI) from the plasmid containing full-length *CgBEM2* and cloned into the SphI-SalI sites of pUC19 plasmid. Using mutagenic primers (listed in supplemental Table S2), the pUC19 plasmid harboring *CgBEM2* fragment was amplified using Phusion High Fidelity DNA Polymerase and ligated. Ultracompetent *Escherichia coli* DH5$\alpha$ cells were used, and the transformants were selected on LB-ampicillin plates. The desired mutation (AGA to GCA) in the pUC19-based plasmid was confirmed by sequencing, and the *CgBEM2* fragment containing this mutation was excised and ligated back into the SphI-SalI sites of pGRB2.2-based plasmid carrying the other half of *CgBEM2*. Sequencing of the resultant plasmid was performed to reconfirm the mutation.

[3] The abbreviations used are: CWI, cell wall integrity; GEF, GDP-GTP exchange factor; GAP, GTPase-activating protein; GTPase, guanosine triphosphatase; CW, Calcofluor white; MB, methylene blue; RhoGAP, Rho1 GTPase-activating protein; PH, pleckstrin homology; R6G, rhodamine 6G; qRT, quantitative real-time.

*Microscopy*—For size measurement, cells were visualized with a Nikon eclipse 80i microscope, and differential interference contrast images were captured using NIS-Elements D3.0 software. To detect nuclei, cells were stained with DAPI (4′,6′-diamino-2-phenylindole) as described previously (10). For Calcofluor white (CW) staining, 1 ml of overnight culture was taken and washed twice with PBS, and cells were suspended in 1 ml of 4% *p*-formaldehyde. After a 2-h incubation at room temperature, cells were washed three times with PBS and resuspended in PBS. One drop of CW (1 mg/ml) and 10% KOH were added to 10 $\mu$l of sample, and cells were visualized by fluorescence microscopy. All images were captured at the same magnification.

*Cell Cycle Analysis by Flow Cytometry*—Flow cytometry for cell cycle analysis was conducted as described previously by Sabatinos and Forsburg (30) with few modifications. Exponentially grown cultures (absorbance = 1.0) were harvested, washed twice with water, and fixed in 1 ml of ice-cold 70% ethanol at 4 °C for 12–16 h. Fixed cells (0.5 absorbance) were washed with 3 ml of 50 mM sodium citrate buffer, suspended in 0.5 ml of 50 mM sodium citrate buffer containing 0.1 mg/ml RNase A, and incubated at 37 °C for 2 h. Propidium iodide was added to a final concentration of 10 $\mu$g/ml. Cells were sonicated for 30 s to avoid doublets, and samples were analyzed by flow cytometry using FACSAria-III (BD Biosciences) with excitation at 488 nm. A minimum of 8000 events were recorded for each sample, and the data were analyzed using DIVA software. The percentages of cells with different DNA contents were determined from the DNA histograms generated with gating.

*Western Analysis*—Logarithmic phase cultures were inoculated at 0.1 absorbance in YPD medium with or without fluconazole and were incubated for 4 h at 30 °C. Cells were washed once with ice-cold water and suspended in 500 $\mu$l of homogenizing buffer (50 mM Tris, pH 7.5, 2 mM EDTA) containing 1 mM phenylmethylsulfonyl fluoride, 10 mM sodium fluoride, 1 mM sodium orthovanadate, and protease inhibitor mixture. Cells were disrupted by glass bead lysis in Fastprep-24 at maximum speed for 60 s five times. Cell debris and unbroken cells were removed by centrifugation at 3000 × *g* at 4 °C for 10 min. Protein was quantified using the BCA protein assay kit as per the supplier instructions. 40 $\mu$g of total protein was run on a 12% SDS-PAGE gel and transferred to PVDF membrane, and the membranes were blocked with 5% w/v fat free milk in TBS-T (50 mM Tris-HCl, pH 7.0, 150 mM NaCl, 0.1% Tween 20) for 1 h at room temperature. Immunoblotting analysis was conducted with an antiphospho-p44/42 MAPK ($Thr^{202}/Tyr^{204}$) primary antibody (Cell Signaling Technology) at a dilution of 1:6000 in TBS-T with 5% w/v fat-free milk for overnight at 4 °C. HRP linked anti-rabbit IgG (Cell Signaling Technology) was used as the secondary antibody, and the blots were developed with ECL plus Western blotting detection system.

*Rho1 Activation Assay*—Rho1 activation was checked using the Rho activation assay biochem kit (Cytoskeleton, BK036) as per the supplier's instructions. Logarithmic phase cells were inoculated in 50 ml of YPD medium to an $A_{600}$ of 0.1, and the desired treatment was given for 4 h. Cells were harvested, washed with ice-cold water, and were suspended in homogenizing buffer. Total protein was isolated as detailed above, and 1 mg of protein was incubated with Rhotekin RhoA binding domain beads for 2 h at 4 °C. The beads were washed once with wash buffer, 2× Laemmli sample buffer was added, and samples were analyzed by Western blotting with a mouse monoclonal anti-RhoA antibody.

*Quantitative Real-time PCR*—Logarithmic phase cultures were inoculated into YPD medium with and without fluconazole (16 $\mu$g/ml) to an $A_{600}$ of 0.1 and grown in a shaker incubator at 30 °C for 4 h. Total RNA was isolated using an acid phenol extraction method, RNA was treated with DNase I to remove any residual DNA, and a total of 500 ng was used to synthesize cDNA by reverse transcriptase enzyme (SuperScript III First-Strand Synthesis System for RT-PCR, Invitrogen). The primers for real time PCR were designed in such a way so as to get amplification products in the size range of 150 to 300 bp. Appropriate primer and cDNA template concentrations were standardized, and real-time PCR was performed in the ABI 7500 real-time PCR machine. The amplification product was run on an agarose gel to confirm the right size amplification. Comparisons were made between the $C_t$ values of fluconazole treated and untreated samples, and -fold difference in expression was calculated.

*Rhodamine 6G Efflux*—Rhodamine 6G efflux was determined as described previously by Emter *et al.* (31) with slight modifications. Briefly, log phase *C. glabrata* cultures ($A_{600}$ = 2.5) were collected, washed with cold water, and suspended in 50 mM HEPES buffer, pH 7.0. To de-energize the cells, 5 mM 2-deoxy-D-glucose was added to the cell suspension. Rhodamine 6G was added to a final concentration of 10 $\mu$M and incubated at room temperature for 2 h. Post-incubation, cells were washed once with 50 mM HEPES, pH 7.0, and divided into two equal parts; one part contained HEPES alone (no energy), and the other provided with 2 mM glucose (energy). Cells were further incubated for 20 min at 30 °C, after which cells were quickly spun down at 5000 × *g* for 2 min. The supernatant was transferred to 96-well flat-bottom microtiter plate, and fluorescence was read using Varioskan Flash spectrofluorimeter (Thermo Scientific). The excitation and the emission wave lengths were 529 and 553 nm (5-nm slit), respectively.

*Other Procedures*—Transformation of *C. glabrata* cells was carried out using the lithium acetate method (10). Cell wall isolation and $\beta$-glucan was measured as described previously (32). van den Hazel's protocol for Rhodamine-6G uptake assay was used (33).

## RESULTS

*A Screen of a C. glabrata Mutant Library Identifies Mutants That Lose Viability upon Exposure to Fluconazole*—In a previous screen for altered fluconazole susceptibility profiles, we had identified catalytic and regulatory subunits of calcium channel, CgCch1 and CgMid1, whose disruption rendered fluconazole fungicidal (10). Expanding upon these earlier findings, we screened 9134 additional *C. glabrata* Tn*7* insertional mutants for the inability to survive fluconazole stress using plate growth assays. Methylene Blue (MB) was used to distinguish live cells from dead cells, as MB is enzymatically broken down to a colorless product by viable cells, whereas non-viable cells accumulate un-degraded MB, resulting in dark blue-colored colonies

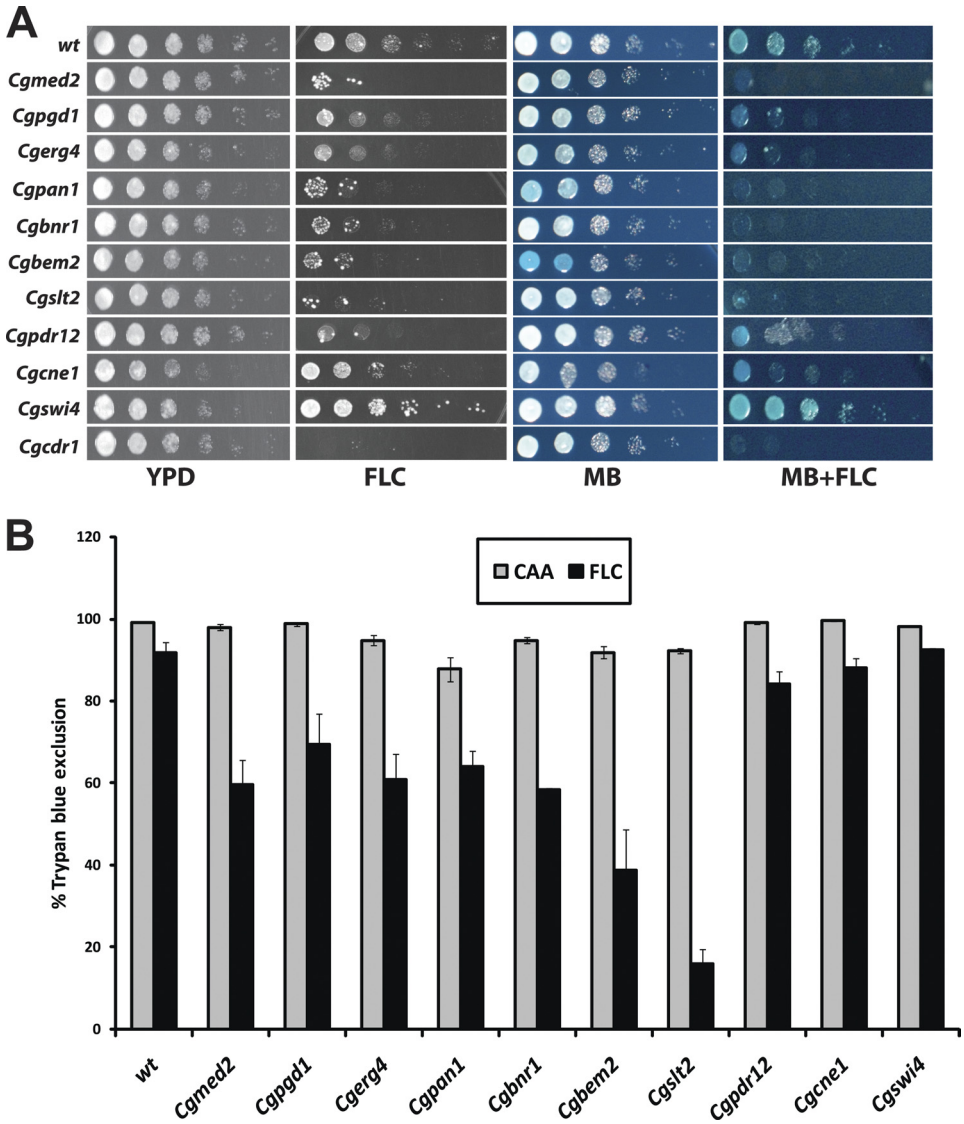


FIGURE 1. ***C. glabrata* mutants defective in RNA polymerase II-dependent transcription and PKC-mediated signaling lose viability in the presence of fluconazole.** *A*, shown are growth profiles of *C. glabrata* fluconazole-sensitive mutants. $A_{600}$ of overnight cultures was normalized to 1.0, and 3 $\mu$l of 10-fold serially diluted cultures were spotted onto YPD plates with or without 16 $\mu$g/ml fluconazole (*FLC*), 0.01% methylene blue (*MB*), or 16 $\mu$g/ml fluconazole, and 0.01% methylene blue (*MB*+*FLC*). Plates were photographed after 24–48 h of growth at 30 °C. *B*, a trypan blue exclusion assay assesses the viability of fluconazole-sensitive mutants in the presence of fluconazole. Cells were grown in CAA medium with or without 128 $\mu$g/ml fluconazole for 24 h, harvested, and washed twice with PBS. Cells were stained with 0.4% trypan blue, and a minimum of total 300 cells (stained (dead) and unstained (viable)) were counted microscopically for each strain. Cell viability data were plotted as the percentage of trypan blue exclusion and represent the mean of three to six independent analyses (±S.E.).

(34). From a set of 9134 mutants screened, a total of 200 mutants showed significant growth inhibition in the presence of 8 $\mu$g/ml fluconazole. Of these, 91 mutants displayed a distinct dark blue color on plates supplemented with 0.01% methylene blue and 16 $\mu$g/ml fluconazole (Fig. 1*A* and data not shown). The blue color of *Cgbem2* colonies on MB plates (Fig. 1*A*) was probably due to an increased cell surface permeability as reported for the *S. cerevisiae bem2* mutant (35). Survival defects of the identified Tn*7* insertion mutants in the presence of fluconazole were independently validated by either trypan blue exclusion/dilution spotting or colony-forming unit assays, and a reproducible loss of viability was observed for 20 mutants in these assays (Fig. 1*B* and data not shown).

Tn*7* insertion mapping and sequencing analysis of these 20 mutants identified multiple insertions in 7 genes (Table 1). Spotting of 24-h fluconazole-treated cultures on YPD medium yielded few viable colonies for these mutants compared with the wild-type (WT) and other fluconazole-sensitive mutants (data not shown). As a control, we showed that a combination of fluconazole and FK506 (calcineurin inhibitor) exerted a fungicidal effect on all *C. glabrata* mutant strains (data not shown). *S. cerevisiae* orthologs of *CgBEM2* and *CgPAN1* are required for organization of actin cytoskeleton (36, 37), whereas *MED2* and *PGD1* are involved in RNA polymerase II-mediated transcription (38, 39). Slt2 and Bnr1 are downstream targets of Pkc1-mediated CWI pathway and Rho-type GTPases family, respectively, in *S. cerevisiae* (40, 41). *CgERG4* encodes C-24 sterol reductase, an enzyme of ergosterol biosynthesis pathway (42). Importantly, none of these genes has directly been implicated in calcium signaling pathway, suggesting the contribution of other signaling cascades in survival of fluconazole stress in *C. glabrata*.

**TABLE 1**
**Mutants identified in a screen for viability loss in the presence of fluconazole**

| Mutant | CAGL-ORF | *S. cerevisiae* ortholog | ORF length | Position (nucleotide) of Tn*7* insertion |
|---|---|---|---|---|
| | | | *Nucleotide* | |
| **RNA polymerase II mediator complex** | | | | |
| *Cgmed2* | *CAGL0C04477g* | *YDL005c* | 1107 | 318 |
| *Cgpgd1* | *CAGL0A01325g* | *YGL025c* | 1434 | 1252 |
| **Ergosterol biosynthesis** | | | | |
| *Cgerg4* | *CAGL0A00429g* | *YGL012w* | 1395 | 170 |
| **Actin cytoskeleton organization** | | | | |
| *Cgpan1* | *CAGL0J01892g* | *YIR006c* | 4125 | 698 |
| **Rho1-mediated signaling** | | | | |
| *Cgbnr1* | *CAGL0H06765g* | *YIL159w* | 3885 | 1747 |
| *Cgbem2* | *CAGL0I06512g* | *YER155c* | 6360 | 1997 |
| *Cgslt2* | *CAGL0J00539g* | *YHR030c* | 1467 | 557 |

Mutants carrying Tn*7* insertions in genes coding for multidrug efflux pumps, CgCdr1 and CgPdr12, showed growth defects in the presence of fluconazole but retained viability (Fig. 1, *A* and *B*). To determine the relationship between PKC signaling components with the observed survival defects in the presence of fluconazole, we selected an additional mutant, identified through another mutant screen in the laboratory, carrying Tn*7* insertion in the *CgSWI4* gene. *SWI4* encodes a DNA binding component of a transcriptional activator Swi4-Swi6 complex, which is under the regulation of Slt2 (43), a key player in imparting tolerance to antifungal agents in *S. cerevisiae* (22). In addition, *Cgcne1*::*Tn7* mutant, previously shown to be fluconazole-sensitive (10), was used as a control. Although *Cgcne1*::*Tn7* and *Cgswi4*::*Tn7* mutants exhibited varied levels of susceptibility to azoles, their survival profiles in the presence of fluconazole were similar to that of the wild type (Figs. 1, *A* and *B*, and 2), thus, validating the results of the mutant library screen.

*Disrupting the Components of Rho GTPase-mediated Signaling Cascade Leads to Sensitivity to Azoles and Cell Wall Damaging Agents*—While this work was in progress, an essential role for PKC signaling in antifungal drug resistance of *C. albicans* via a circuitry composed of Mkc1, calcineurin, and Hsp90 was reported (22). Of the seven genes identified in our mutant screen, three genes encode putative constituents of Rho GTPases-mediated signaling pathways (23, 26, 44). *CgBEM2* and *CgSLT2* code for a RhoGAP and a serine/threonine MAPK of CgPkc1-mediated CWI cascade, respectively (supplemental Table S3), whereas *CgBNR1* encodes a formin protein. In *S. cerevisiae*, Bni1, a homolog of Bnr1, is a target of an essential small GTPase Rho1 (45).

To examine if the CgPkc1-mediated CWI pathway regulates antifungal drug susceptibility in *C. glabrata*, we conducted phenotypic profiling analyses on all fluconazole-sensitive mutants. Mutants potentially disrupted for Rho signaling exhibited sensitivity to all azole drugs and cell wall damaging agents including caffeine, Calcofluor white (CW), and Congo red (Fig. 2 and data not shown). Additionally, growth of the *Cgbem2* mutant was inhibited at 42 °C, and osmotic stabilization with sorbitol could partially rescue the thermal stress sensitivity and cell wall-related defects (Fig. 2). In contrast, sorbitol completely suppressed the temperature sensitivity of the *Cgpan1* mutant. The *Cgslt2* mutant was neither temperature-sensitive for growth at 37 °C nor at 42 °C; this is in contrast to an earlier study reporting decreased tolerance of Cg*slt2*Δ mutants to elevated temperature (46). This discrepancy could be due to differences in the genetic background of the parental strains. The *Cgbnr1* mutant displayed reduced susceptibility to cell wall stress agents (Fig. 2). Importantly, no altered sensitivity to a polyene antifungal amphotericin B was observed for any of the mutants (data not shown).

Mutants defective in RNA polymerase II-mediated transcription and multidrug efflux pumps displayed sensitivity to only azoles (Fig. 2). Additionally, *Cgcne1* did not grow at 42 °C, whereas growth of *Cgswi4* mutant was strongly attenuated in the presence of cell wall-damaging agents, and sorbitol addition restored the cell-wall related defects (Fig. 2). Surprisingly, *Cgswi4* mutant showed resistance to all the three azoles tested, fluconazole, clotrimazole, and ketoconazole (Fig. 2 and data not shown); the molecular basis of this phenotype is not clear and warrants further investigation. *Cgerg4*, *Cgpan1*, *Cgbnr1*, and *Cgcne1* mutants were exquisitely sensitive to cell membrane-disrupting agent SDS (Fig. 2). Altogether, the phenotypic profiling data suggest that components of CWI pathway, actin cytoskeleton organization machinery, sterol biosynthesis, and mediator complex, are required for tolerance/resistance to the azole class of antifungals in *C. glabrata*.

*Disruption of CgBEM2 Causes Defects in Bud Emergence, Viability Loss during Fluconazole Stress, and Cell Wall-related Phenotypes*—To investigate the role of *CgBEM2*, *CgPAN1*, and *CgSLT2* in the susceptibility of *C. glabrata* toward azoles, we sought to generate knock-out strains for these genes. Although we were able to disrupt *CgBEM2* and *CgSLT2* with the dominant nourseothricin resistance marker (*nat1*), our attempts to delete *CgPAN1* were unsuccessful with both one-step and two-step disruption methodologies. This led us consider the possibility that *CgPAN1* is essential for viability in *C. glabrata.* Plasmid shuffling experiments demonstrated that *C. glabrata* cells lacking *CgPAN1* were inviable (data not shown). Notably, *PAN1* is an essential gene in *S. cerevisiae* (47).

Next, phenotypic characterization of *Cgbem2*Δ and *Cgslt2*Δ mutants revealed a growth defect for *Cgbem2*Δ strains in YPD medium (doubling time = 95 min) compared with the WT strain (doubling time = 72 min) (Fig. 3*A*). Time-course analysis confirmed the sensitivity to fluconazole and high temperature for *Cgbem2*Δ and to fluconazole for *Cgslt2*Δ mutant (Fig. 3*A*). Furthermore, trypan blue exclusion assays to assess the fungicidal nature of fluconazole in these mutant backgrounds showed that whereas 90–95% of *C. glabrata* WT cells remained

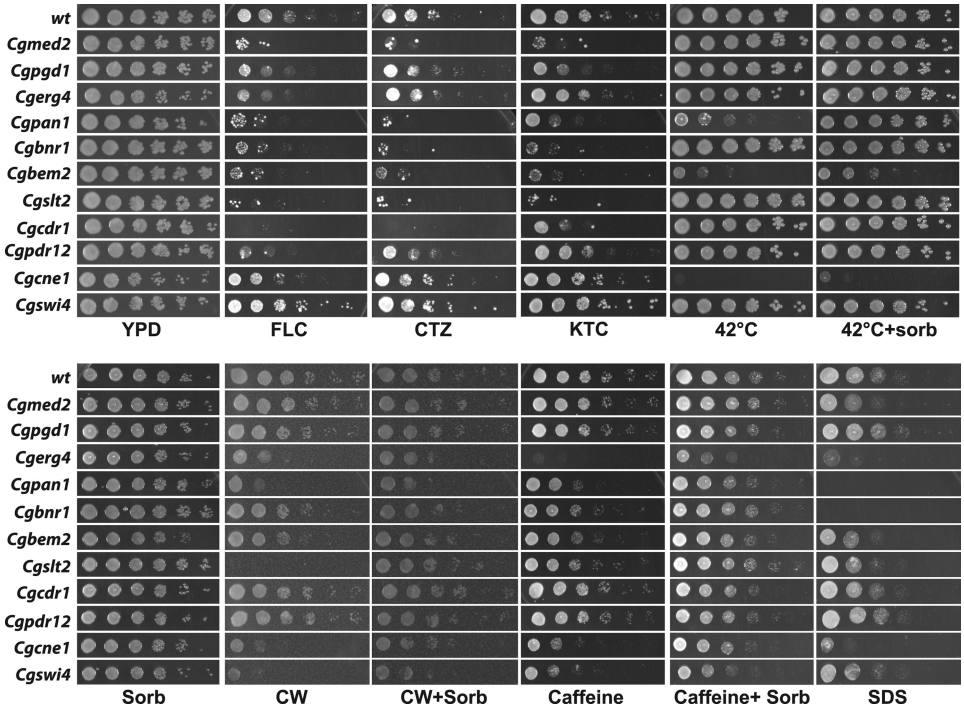


FIGURE 2. **Disruption of Rho GTPase-mediated signaling leads to susceptibility to azoles and cell wall stress agents.** Equal volumes of 10-fold serial dilutions of wild-type and mutant cultures were spotted onto YPD plates containing different stress agents at the following concentrations and growth was scored after 48 h: fluconazole (*FLC*, 16 $\mu$g/ml), clotrimazole (*CTZ*, 15 $\mu$g/ml), ketoconazole (*KTC*, 10 $\mu$g/ml), caffeine (10 mM), Calcofluor white (*CW*, 1.5 mg/ml), sorbitol (*Sorb*, 1 M), SDS (0.05%), and thermal stress (42 °C).

viable after 24 h of treatment with fluconazole, *Cgbem2*Δ and *Cgslt2*Δ exhibited a survival rate of 29 and 48%, respectively (supplemental Fig. S1). Similar to the Tn*7* insertional mutant phenotypes, *Cgbem2*Δ and *Cgslt2*Δ strains exhibited sensitivity to other azole compounds and cell wall stress agents (data not shown). Importantly, no growth inhibition was observed on plates supplemented with amphotericin B, sodium chloride, calcium chloride, and terbinafine for these deletion strains (data not shown).

In *S. cerevisiae*, cells lacking Bem2 display defects in actin polarity, bud-site selection, cell wall integrity, and sensitivity to antifungals (35, 36). Accordingly, microscopic examination of *Cgbem2*Δ cells revealed defects in bud emergence and variations in size and morphology. Their size ranged from 4 to 7 $\mu$m, whereas the mean size of wild-type cells was 3.9 $\mu$m. A typical logarithmic-phase culture of *Cgbem2*Δ accumulated a high percentage (20–25%) of the cells as oversized, large, un/small-budded cells (Fig. 3, *B* and C, and data not shown). DAPI staining of these cells revealed that each enlarged cell possessed multiple nuclei, consistent with bud emergence defects (Fig. 3*B* and data not shown). To test whether these cytological defects are associated with defects in cell surface growth, we labeled cells with the chitin-specific dye Calcofluor white. Although the chitin staining was restricted mostly to bud-scars in WT cells, bright and dispersed staining indicating delocalized chitin deposition was observed for *Cgbem2*Δ cells (Fig. 3*C*). These data suggest that disruption of *CgBEM2* results in enlarged, multinucleate cells with delocalized cell surface growth in *C. glabrata.* Importantly, both fluconazole and temperature sensitivity of the *Cgbem2*Δ strain was complemented by ectopic expression of *CgBEM2* (supplemental Figs. S1 and S2). Expression of *CgSLT2* restored the growth defect and viability loss of *Cgslt2*Δ in the presence of fluconazole and clotrimazole (supplemental Figs. S1 and S2). Notably, expression of *CgSLT2* and *CgRHO1* could not rescue the fluconazole and temperature susceptibility of *Cgbem2*Δ mutant (supplemental Fig. S2); however, azole sensitivity of *Cgslt2*Δ was partially restored by plasmid expressing *CgRHO1* (supplemental Fig. S2).

*Cgbem2*Δ *Cells Display Enhanced Polyploidy upon Fluconazole Exposure*—Budding and cell cycle-related defects are characteristic features of *Cgbem2*Δ cells. To better understand the molecular basis underlying viability loss of *Cgbem2*Δ in fluconazole-supplemented medium, we performed cell cycle analysis on logarithmic phase cells grown either in the presence or absence of fluconazole. As shown in Fig. 4, WT cells follow regular cell cycle events maintaining a similar distribution of S-, $G_1$- and $G_2$-phase cells during a 4-h treatment with fluconazole. In contrast, for *Cgbem2*Δ cells there was a decrease in the cell number (6%) with S-phase DNA content and in $G_2$/M phase (39%) compared with the 14 and 54% in WT cells, respectively (Fig. 4). A concomitant increase in cell population with polyploidy (40%) was observed for *Cgbem2*Δ compared with the 8 and 14% polyploid cells observed in fluconazole-treated WT cells and untreated mutant cultures, respectively (Fig. 4), suggesting that the incapacity of *Cgbem2*Δ to survive fluconazole stress is in part due to altered progression through the cell cycle. Notably, a *Cgbem2*Δ-reconstituted strain restored wild-type-like cell cycle profiles upon fluconazole exposure (Fig. 4). No increase in polyploids was seen for the *Cgslt2*Δ mutant (data not shown). Importantly, all strains were able to arrest in the S phase of the cell cycle upon hydroxyurea (blocks replication fork progression) treatment (data not shown). Because Bem2 in

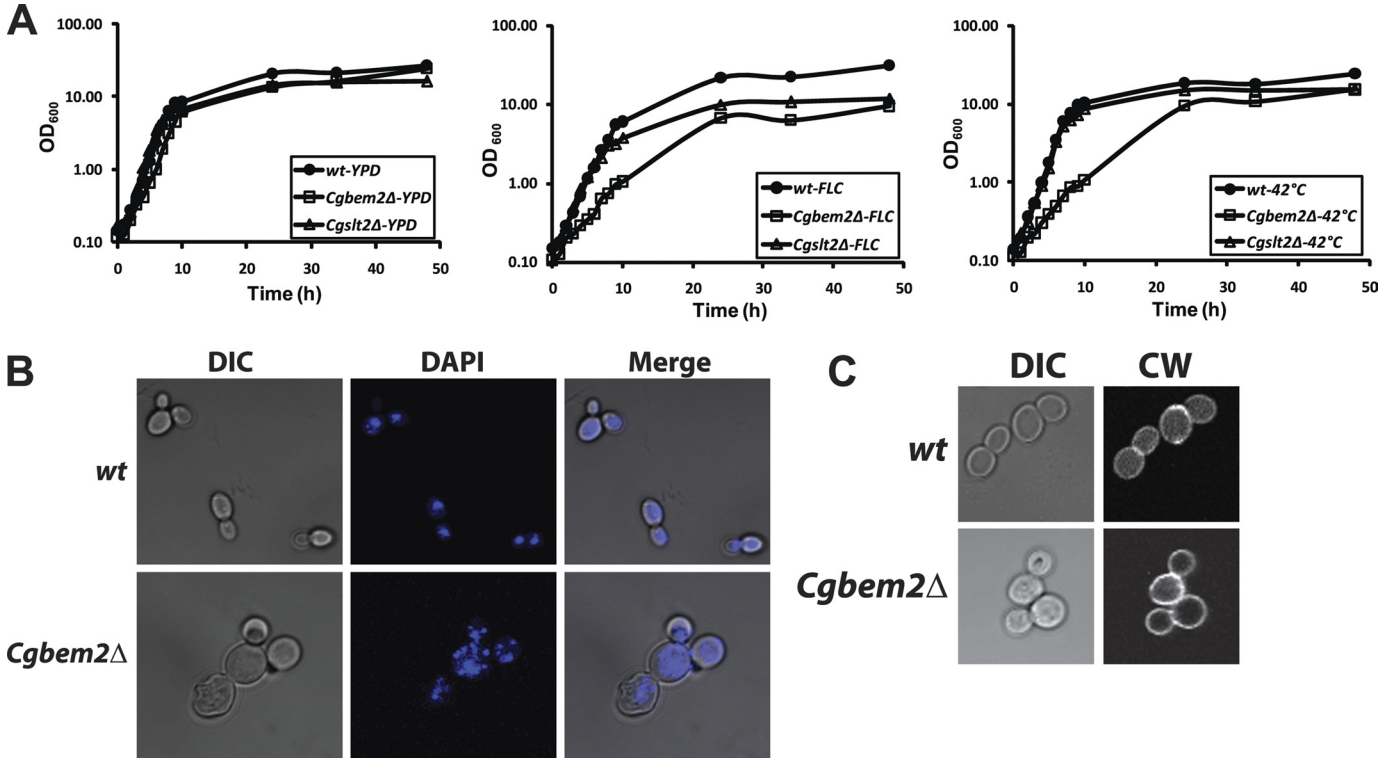


FIGURE 3. **Disruption of *CgBEM2* results in fluconazole and thermal stress sensitivity and bud-emergence defects.** *A*, shown is growth curve analysis of WT, *Cgbem2*Δ, and *Cgslt2*Δ mutants in YPD medium at 30 and 42 °C and in YPD medium containing 16 μg/ml fluconazole. Absorbance at 600 nm was monitored over a 48-h time course at the indicated time intervals. Data are represented as mean values of two independent growth analyses. *B*, differential interference contrast (*DIC*) and fluorescence confocal images of DAPI stained *Cgbem2*Δ mutant reveal enlarged, multi-nucleated cells. Logarithmic phase *C. glabrata* cells were fixed, stained with 0.2 mg/ml DAPI for 40 min, and visualized using confocal microscopy. *C*, DIC and fluorescence confocal images of CW (1 mg/ml)-stained *Cgbem2*Δ mutant display diffused chitin staining, indicating delocalized cell surface growth. All the growth assays were performed at 30 °C unless mentioned otherwise.

*S. cerevisiae* is required for the morphogenesis checkpoint, which delays mitosis in response to impaired actin organization and bud formation, thereby coupling cell cycle progression with proper bud formation (48), it is plausible that an increase in polyploid population in *Cgbem2*Δ cells upon fluconazole exposure may reflect an exacerbated morphogenesis checkpoint defect.

*CgPkc1-mediated Signaling Pathway Is Constitutively Active in Cgbem2*Δ *Cells*—CgBem2 is a GAP domain-containing protein whose ortholog in *S. cerevisiae* negatively regulates Rho1 and is implicated in cell polarity and morphogenesis, cell wall integrity, and actin cytoskeleton biogenesis (24, 27, 28).

To investigate if CgBem2 functions as a negative regulator of CgRho1, we directly measured the activation status of CgRho1 via affinity pulldown assays in WT and *Cgbem2*Δ cells grown under different conditions. Beads coated with RhoA binding domain of the RhoA effector protein, Rhotekin, which binds to only the active, GTP-bound RhoA form, were used, and a faint band corresponding to 23-kDa CgRho1 was observed in YPD-cultured WT cells. Growth in the presence of cell wall stress agent caffeine resulted in higher levels of GTP-bound form of CgRho1 in WT cells (Fig. 5*A* and data not shown). In contrast, YPD grown cultures of *Cgbem2*Δ possessed higher amount of active GTPase, and a further significant increase in GTP-bound form of CgRho1 was observed upon cell wall stress (Fig. 5*A*). Notably, levels of total Rho1 were nearly identical across all samples (Fig. 5*A*). Activation of Rho-like small GTPases leads to membrane association. Similarly, fluconazole treatment led to an ~2-fold increase in the CgRho1 levels in the membrane fractions of WT cells (supplemental Fig. S3); however, we were unable to observe a consistent activation of Rho1 GTPase by RhoA binding domain pulldown assays (data not shown). YPD-cultured *Cgbem2*Δ cells displayed an ~3-fold higher amount of membrane-associated CgRho1 (supplemental Fig. S3), reinforcing the result that CgBem2 negatively regulates CgRho1, and mutants deleted for *CgBEM2* contain higher levels of constitutively active CgRho1.

To verify that higher levels of the GTP-bound form of CgRho1 resulted in the activation of CgPkc1-mediated CWI pathway in *Cgbem2* mutants, we monitored the phosphorylation state of CgSlt2 (an indicator of Pkc1 activation) by using an antibody that detects only the doubly phosphorylated (active) form of the protein. Consistent with a recent study (22), a band of 56 kDa, corresponding to the phosphorylated CgSlt2, appeared in WT cell extracts upon fluconazole exposure, representing an activated Pkc1-MAPK cascade (Fig. 5*B*). Additionally, we observed approximately a 3-fold increase in total CgSlt2 levels upon drug exposure (Fig. 5*B*). Compared with the WT cells, basal levels of CgSlt2 phosphorylation were elevated in the *Cgbem2*Δ strain, and a further 2-fold induction was seen upon drug exposure (Fig. 5*B*). As expected, no band corresponding to CgSlt2 was detected in the *Cgslt2*Δ mutant (data not shown). Similar profiles of CgSlt2 expression and phosphorylation were observed in response to caffeine-induced cell wall stress (data

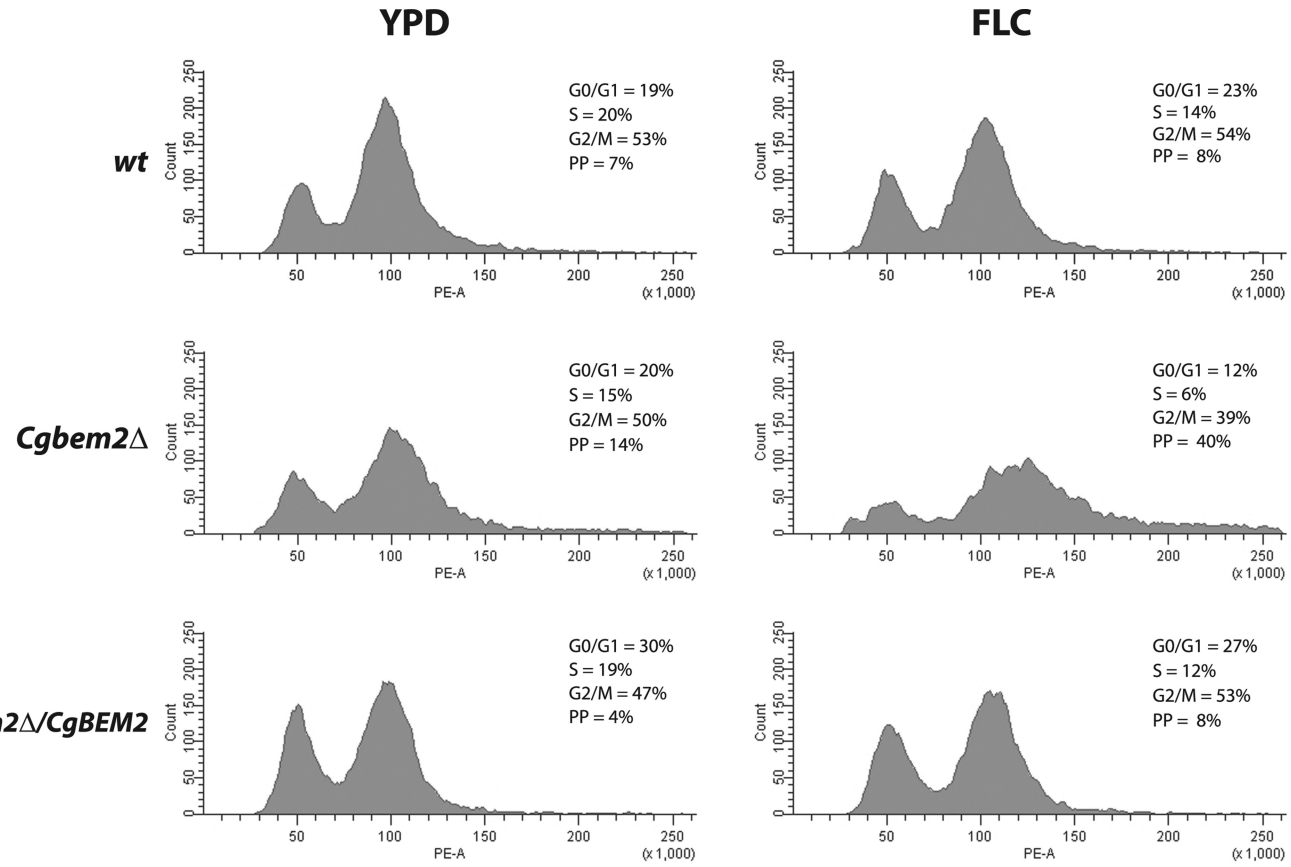


FIGURE 4. **Flow cytometric analyses of propidium iodide-stained wild-type, *Cgbem2*Δ, and *Cgbem2*Δ/*CgBEM2* cells.** Logarithmic phase *C. glabrata* cells were fixed with 70% ethanol, and flow cytometric analysis of DNA contents was carried out as described under "Experimental Procedures." The *x* axis represents relative DNA content. The *left-most peak* represents the G1 population, and the *right-most peak* represents the G2 population. *PP* refers to polyploid population. Data shown are from one experiment and are representative of three independent experiments. *FLC*, fluconazole.

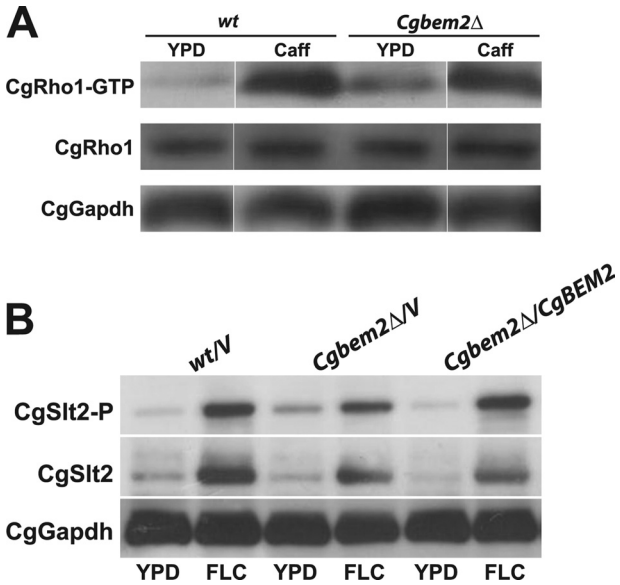


FIGURE 5. **CgPkc1-mediated signaling cascade is constitutively active in *Cgbem2*Δ mutant.** *A*, shown is a Western blot analysis detecting the GTP-bound form of CgRho1 on *C. glabrata* cells grown in the presence of 10 mM caffeine (*Caff*) for 4 h. Experimental details are outlined under "Experimental Procedures." *B*, shown is a Western blot analysis detecting the total and phospho form of CgSlt2 on *C. glabrata* cells grown either in YPD or YPD medium containing 16 μg/ml fluconazole (*FLC*) for 4 h. Activation of CgSlt2 was examined by probing the blot with anti-phospho-p44/42 MAPK antibody that recognizes the dual-phosphorylated form of CgSlt2. CgGapdh was used as a loading control.

not shown). Furthermore, ectopic expression of *CgBEM2* in *Cgbem2*Δ mutant resulted in phosphorylated CgSlt2 levels comparable with those of the WT cells (Fig. 5*B*). Collectively, these data indicate that Rho1-dependent CgPkc1-mediated CWI signaling cascade is constitutively active in *C. glabrata* mutants lacking CgBem2. Intriguingly, increasing the dosage of neither CgSlt2 nor CgRho1 had any effect on the thermal and azole stress sensitivity of *Cgbem2*Δ mutant (supplemental Fig. S2); the basis for this observation is not clear. Because Western analysis revealed higher basal levels of Rho1-GTP and CgSlt2 in activated state in *Cgbem2*Δ cells (Fig. 5*B*, supplemental Figs. S3 and S4), increasing the copy number of either protein should result in exacerbation of *Cgbem2*Δ mutant phenotypes. However, this is not what we observed. A likely explanation for this is the feedback inhibition, and/or controlled cycling between the GTP- and GDP-bound forms of CgRho1 may be critical for proper activation of the CgPkc1-mediated signal transduction cascade.

*GAP Domain of CgBem2 Is Required for Azole Tolerance*—CgBem2, a Rho GTPase activating protein composed of 2119 amino acid residues, is encoded by ORF *CAGL0I06512g* (Génolevures). *In silico* structural analysis predicted CgBem2 to possess a Ras-GEF, a RasGEF-N, a PH (pleckstrin homology), and a RhoGAP domain (Fig. 6*A*). In the screen for altered fluconazole survival profiles, three mutants carrying Tn*7* insertion in *CgBEM2* were identified, and the Tn*7* insertion was

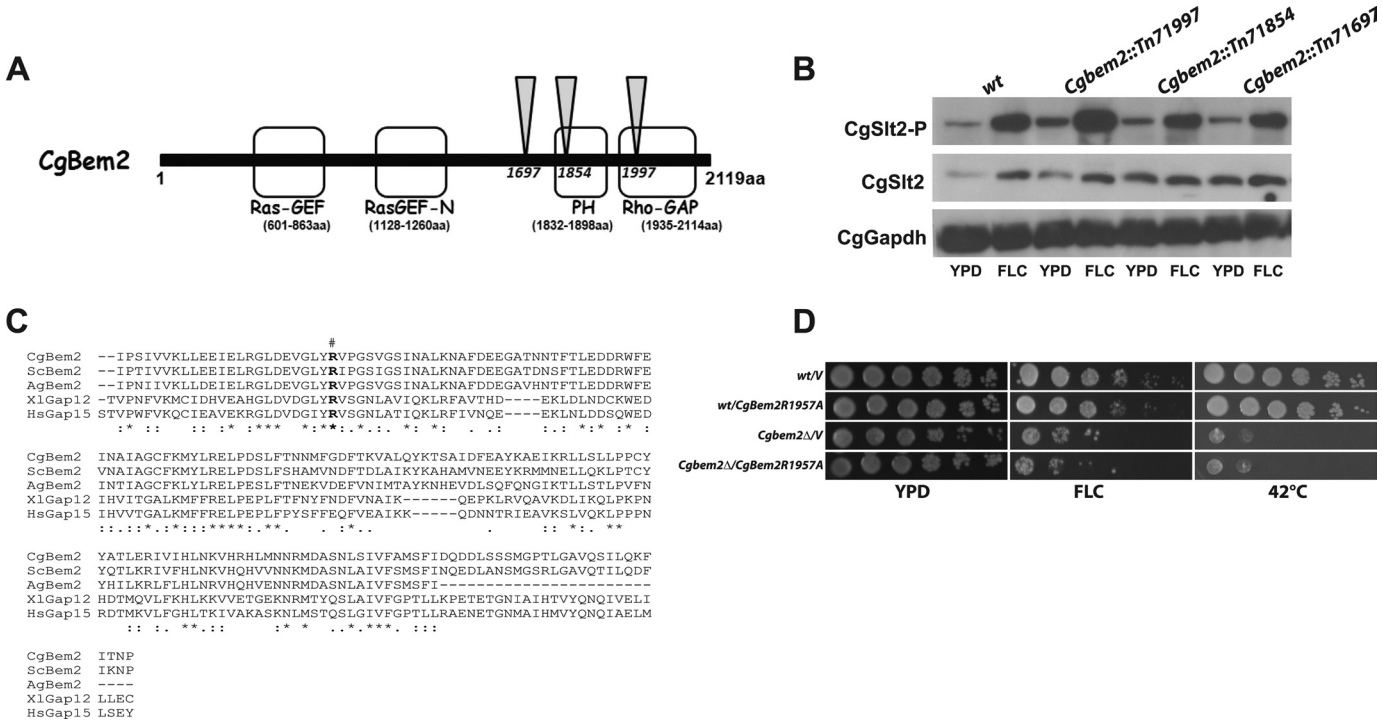


FIGURE 6. **RhoGAP domain of CgBem2 is required for fluconazole tolerance.** *A*, shown is a schematic illustration of the predicted domains of CgBem2 protein. *Inverted triangles* indicate the positions of Tn7 insertions in identified *Cgbem2* mutants. The diagram is not drawn to scale. *aa*, amino acids. *B*, shown is a Western blot analysis detecting the total and phospho form of CgSlt2 on *Cgbem2*::*Tn7* insertional mutants as indicated in the Fig. 5*B* legend. *FLC*, fluconazole. *C*, shown is a sequence comparison of the GAP domain of Rho-GAP proteins. A multiple alignment was calculated with ClustalW by using protein sequences of *C. glabrata* Bem2 (CgBem2), *S. cerevisiae* Bem2 (ScBem2), *Ashbya gossypii* Bem2 (AgBem2), *Xenopus laevis* RhoGAP protein 12 (XlGap12), and *Homo sapiens* RhoGAP protein 15 (HsGap15). The putative catalytic arginine residue is *highlighted* in *bold* and is also marked with the *hash symbol*. *Stars* indicate identical amino acids, and *colons* and *dots* represent similar amino acids. *D*, shown are growth profiles of the wild-type and *Cgbem2*Δ strain harboring either empty vector pRK74 or plasmid expressing mutated CgBem2R1957A in the presence of fluconazole and thermal stress (42 °C).

mapped to the region upstream of PH domain, to the PH domain, and to the RhoGAP domain in these mutants (Fig. 6*A*). All these mutants showed sensitivity to fluconazole and elevated temperature (supplemental Fig. S5) and a constitutively active CgSlt2 (Fig. 6*B*), indicating that CgBem2 protein is required for response to azole antifungals and for controlled activation of CgPkc1-mediated signaling.

Furthermore, to investigate the precise role of the GAP domain in enhanced fluconazole susceptibility of *Cgbem2* mutants, we replaced a highly conserved, catalytic arginine residue (Fig. 6*C*), present at 1957 position in the GAP domain of CgBem2, with alanine by site-directed mutagenesis and tested the ability of this mutant protein (CgBem2R1957A) to complement the fluconazole, thermal, and cell wall stress sensitivity. CgBem2R1957A expression could neither rescue the growth defects of *Cgbem2*Δ cells nor did its expression in WT cells lead to elevated susceptibility to azoles and high temperature (Fig. 6*D* and data not shown). Additionally, the levels of phosphorylated CgSlt2 remained unchanged in WT and *Cgbem2*Δ cells expressing mutated CgBem2 protein compared with the untransformed cultures (supplemental Fig. S4). Our attempts to examine CgBem2 levels by Western were unsuccessful due to the cross-reactivity of the antibody raised against an N-terminal peptide of CgBem2 (data not shown); however, qRT-PCR revealed that the mutant allele was expressed at levels comparable to those of the wild-type *CgBEM2* in both WT and *Cgbem2*Δ transformants (data not shown). Altogether, these results indicate a requirement for a functional GAP domain for the role of CgBem2 in conferring tolerance to thermal, cell wall, and azole stress in *C. glabrata*.

*Viability Loss of Cgbem2*Δ *Mutant upon Fluconazole Treatment Is Partially Rescued by Inhibition of CgPkc1 Signaling*—Because CgPkc1-mediated signaling was constitutively active in *Cgbem2* mutants, it was important to determine whether there is a link between survival of fluconazole stress and deregulated CgRho1-Pkc1 signal transduction cascade.

To address this, we first investigated the physiological consequences of a constitutively active CgPkc1 signaling. In *S. cerevisiae*, activation of the Pkc1-mediated CWI pathway leads to an increased synthesis of β-glucan and enhanced expression of Rlm1 and Swi4 targets including Fks2 (49, 50). To examine whether CgBem2 controls 1,3-β-glucan synthase activity, we measured β-glucan levels in WT and *Cgbem2*Δ cells grown in the presence or absence of fluconazole. A 20% increase in β-glucan amount was seen in drug-treated WT cells (Fig. 7*A*). In contrast, *Cgbem2*Δ cells displayed 50% higher β-glucan content in their cell walls even under standard growth conditions, and a modest reduction was seen in fluconazole-cultured cells (Fig. 7*A*), implying an inability to further activate CgFks2 in response to the drug treatment and an imbalance in the polysaccharide composition of cell wall. Expression of *CgBEM2* in *Cgbem2*Δ cells led to wild-type β-glucan levels (Fig. 7*A*), indicating that a constitutively activated CgPkc1-mediated CWI pathway leads to increased β-glucan levels in the cell wall of *Cgbem2*Δ mutant.

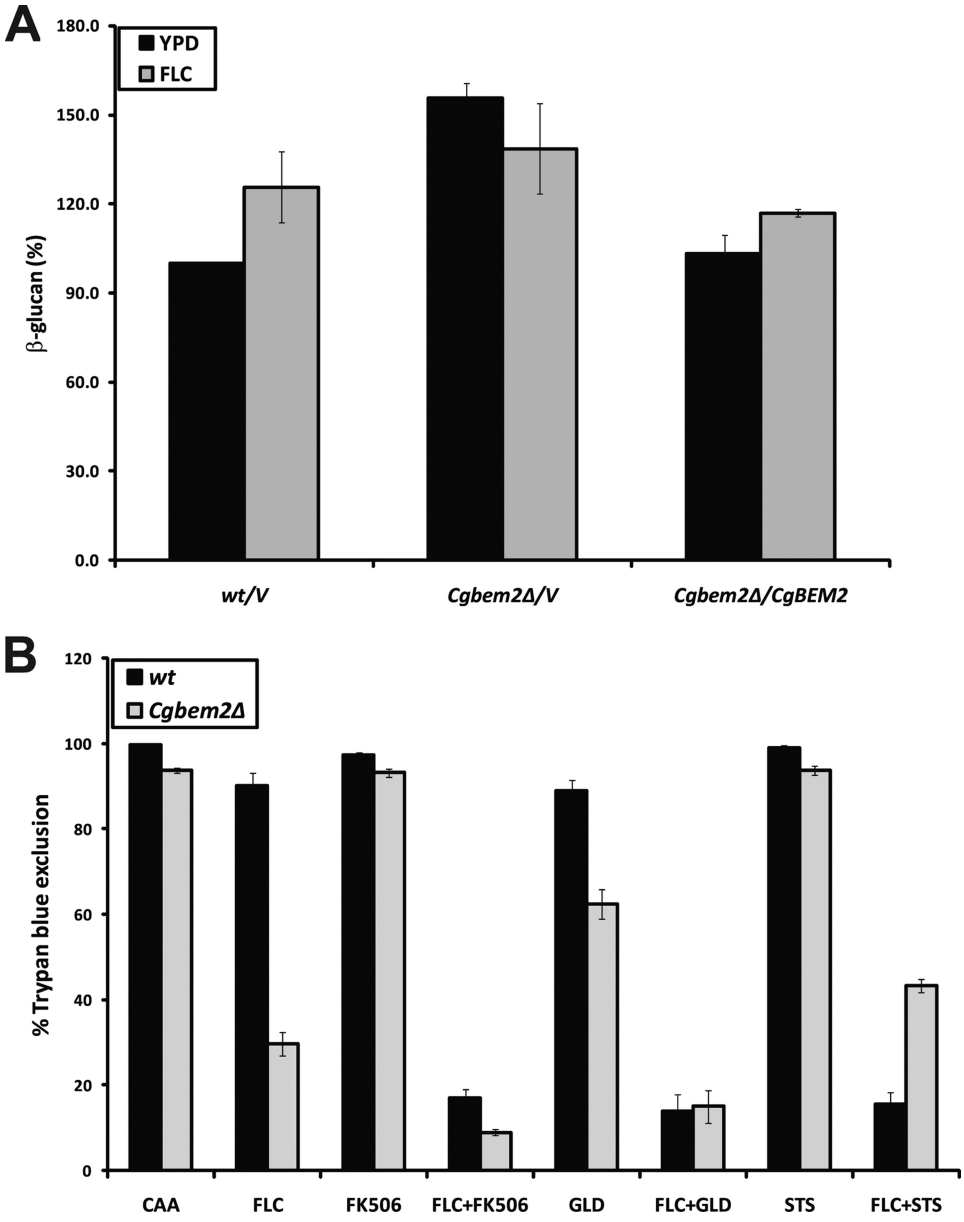


FIGURE 7. **Fluconazole-induced viability loss in *Cgbem2*Δ mutant is partially rescued by inhibition of CgPkc1 signaling.** *A*, β-glucan content of wild-type and *Cgbem2* mutants grown either in YPD or in YPD medium containing 16 μg/ml fluconazole (*FLC*) was determined as described previously (32) and was expressed as μg of glucan/mg of dry weight of cell wall. Total amount of β-glucan quantified from YPD grown wild-type cells was normalized to 100%, and data presented are relative to the β-glucan levels in WT cell wall under standard growth conditions. Cell wall analysis was independently carried out three-four times, and *error bars* represent S.E. *B*, the fungicidal nature of fluconazole was assessed by growing cultures for 24 h in the presence of 2 μg/ml FK506, 25 μM geldanamycin, and 2 μg/ml staurosporine in medium with or without 128 μg/ml fluconazole followed by viability assessment by trypan blue exclusion assay as outlined in Fig. 1*B* legend. Data represent the means ± S.E. of three-five independent experiments.

Next, we tested whether inhibition of PKC signaling could rescue fluconazole-induced cell death in *Cgbem2*Δ mutant. For WT cells in medium containing fluconazole, the addition of the PKC inhibitor staurosporine reduced the recoverable viable cells from 90 to 15% (Fig. 7*B*). In contrast, the *Cgbem2*Δ cells grew better in medium containing fluconazole and staurosporine than in medium containing fluconazole alone. Furthermore, the addition of staurosporine strikingly increased viability of fluconazole-treated *Cgbem2*Δ cells (43% viability for fluconazole- and staurosporine-treated compared with 29% survival for fluconazole alone) (Fig. 7*B*). As a control, growth profiles of WT and *Cgbem2*Δ mutant were monitored in the presence of geldanamycin (Hsp90 inhibitor) and FK506 (calcineurin signaling inhibitor) either alone or in combination with fluconazole. FK506 has previously been shown to act synergistically with fluconazole in *C. glabrata* (10). Consistent with those results, 9% of *Cgbem2*Δ cells could exclude trypan blue in the presence of FK506 and fluconazole compared with 29% in the presence of fluconazole alone (Fig. 7*B*). A synergistic cidal effect of fluconazole was observed with geldanamycin in WT and *Cgbem2*Δ cells with both survival rates being ~15% (Fig. 7*B*). Interestingly, *Cgbem2*Δ cells exhibited a modest survival defect in medium containing geldanamycin alone (Fig. 7*B*), indicating a cross-talk between PKC-mediated CWI and Hsp90-mediated cell survival in *C. glabrata*. Collectively,

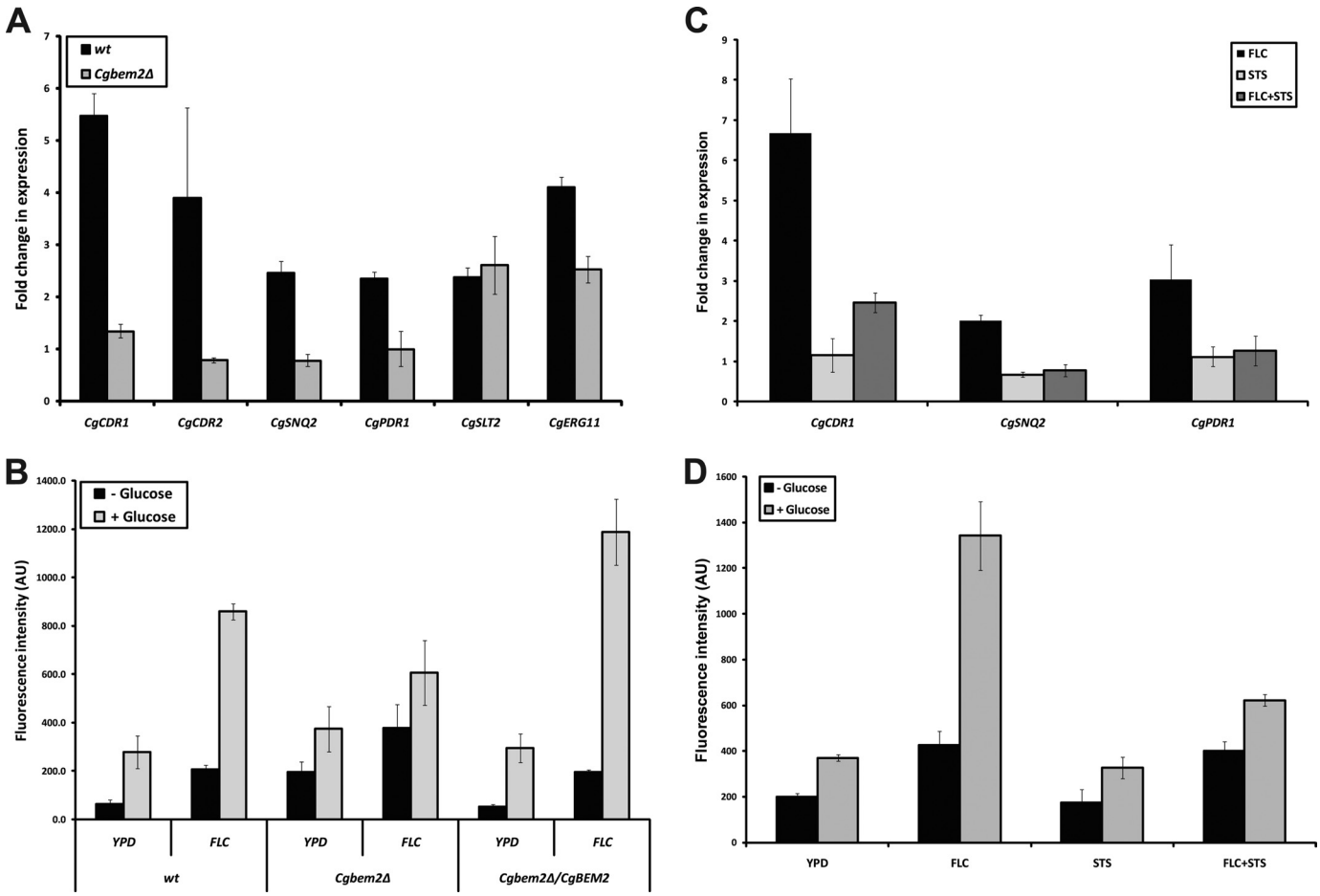


FIGURE 8. **CgBEM2 is required for activation of multidrug efflux pumps in response to fluconazole.** *A*, shown are qRT-PCR analyses of *CgCDR1*, *CgCDR2*, *CgSNQ2*, *CgPDR1*, *CgSLT2*, and *CgERG11* genes on cells grown in 16 $\mu$g/ml fluconazole for 4 h. Assays were performed in duplicate with SYBR® Green dye using ABI PRISM® 7500 Sequence Detection System. Data were normalized to an internal *CgGAPDH* mRNA control, and the relative changes in transcriptional level upon fluconazole exposure were calculated as a ratio of the transcript levels of treated cells *versus* non-treated cells using the $2^{-\Delta\Delta CT}$ method. Data represent the means of 3–5 independent experiments ± S.E. *B*, efflux of R6G in wild-type and mutant cultures grown for 4 h in the absence or presence of 16 $\mu$g/ml fluconazole (*FLC*). De-energized cells were incubated with 10 $\mu$M R6G at 30 °C for 2 h, and cells were rapidly harvested. Active efflux of R6G was initiated by the addition of 2 mM glucose to energy-starved, R6G-preloaded cells, and the extracellular concentration of R6G in the supernatant was determined fluorometrically 20 min post-glucose addition. Data are from three to five independent analyses ± S.E. *AU* represents arbitrary units. *C*, shown are qRT-PCR analyses of *CgCDR1*, *CgSNQ2*, and *CgPDR1* genes on wild-type cells grown for 4 h under different conditions. Fluconazole and staurosporine (*STS*) were used at a concentration of 16 and 1 $\mu$g/ml, respectively. Assays were performed in duplicate as described in *A*. Data represent the mean ± S.E. of three to four independent experiments. *D*, efflux of R6G in wild-type cells grown for 4 h under different conditions was assessed as described in *B* is shown. Fluconazole and staurosporine were used at the concentration of 16 and 1 $\mu$g/ml, respectively. Data represent the mean ± S.E. of three independent experiments.

these results suggest that the inability of *Cgbem2*Δ cells to survive fluconazole stress is due to a hyperactivated CgPkc1-mediated CWI pathway.

*CgBEM2 Is Required for Activation of Multidrug Efflux Pumps in Response to Fluconazole*—To decipher the molecular mechanism for enhanced susceptibility of *Cgbem2*Δ strain toward fluconazole, we examined the expression of five genes that have been reported to contribute to azole resistance in *C. glabrata* in the mutant background. These five genes, *CgCDR1*, *CgCDR2*, and *CgSNQ2*, *CgPDR1* and *CgERG11*, code for plasma membrane ATP-binding cassette transporters, zinc finger transcriptional regulator of pleiotropic drug resistance genes, and lanosterol 14-$\alpha$-demethylase (target of fluconazole), respectively (7, 9, 11, 12). Consistent with earlier reports, wild-type cells responded to fluconazole exposure by elevating the expression of genes coding for drug transporters (Cdr1 and Cdr2) by 4–6-fold (Fig. 8*A*). About 2.5-fold induction was seen in the expression levels of the third drug transporter, CgSnq2, and of the transcriptional factor CgPdr1 (Fig. 8*A*). In contrast, fluconazole-treated cells of *Cgbem2*Δ showed neither induction of the genes coding for ABC transporters nor for the transcriptional regulator (Fig. 8*A*). Notably, fluconazole induced the transcriptional activation of *CgERG11* (3–4-fold) and *CgSLT2* (2.5-fold) in both WT and *Cgbem2*Δ cells (Fig. 8*A*), indicating that cells respond to drug exposure by elevating the expression of its target enzyme and a MAPK. *CgSLT2* has previously been reported to be transcriptionally up-regulated in response to an echinocandin drug, caspofungin (51). A 2-fold increase in *CgFKS2* expression levels in both WT and *Cgbem2*Δ upon fluconazole exposure was also observed (data not shown). Steady-state RNA levels of *CgCDR1*, *CgCDR2*, *CgSNQ2*, and *CgPDR1* in the absence of drug were approximately equivalent in all strains (data not shown), thus ruling out global transcriptional defects in *Cgbem2*Δ mutant. Importantly, drug-treated cultures of reconstituted *Cgbem2*Δ/*CgBEM2* strain displayed up-regulation of *CDR* genes similar to that of the WT cells (data not shown).

These data indicate that CgBem2 is required for the transcriptional activation of the genes coding for ABC transporters and their transcriptional regulator upon fluconazole exposure.

Next, to corroborate the above qPCR results, we measured the efflux in different strain backgrounds of a fluorescent dye rhodamine 6G (R6G), which is specifically extruded by CgCdr1 in an ATP-dependent manner (52). As shown in Fig. 8*B*, WT cells showed a 4-fold energy-dependent enhanced efflux of R6G upon fluconazole treatment. A *C. glabrata* mutant carrying a Tn7 insertion in the *CDR1* gene was used as a negative control, and no significant increase in R6G efflux was seen upon drug exposure in response to glucose pulse (data not shown). Quantitative uptake and accumulation assays revealed that *Cgbem2* mutants take up R6G at a higher rate than the WT cells (supplemental Fig. S6 and data not shown); however, energy-dependent extrusion of R6G was not significantly elevated after fluconazole treatment in *Cgbem2*Δ mutant (Fig. 8*B*). Collectively, the qRT-PCR and R6G efflux analyses demonstrate that CgBem2 plays a crucial role in the regulation of activity of drug efflux pumps, and defective regulation of these transporters may partially explain the increased fluconazole susceptibility associated with *CgBEM2* disruption.

Last, to investigate the possibility of whether CgPkc1-mediated signaling is required for the activation of multidrug transporters upon fluconazole exposure, we conducted qRT-PCR and R6G efflux analyses on staurosporine-treated wild-type cells. As shown in Fig. 8*C*, co-incubation with fluconazole and staurosporine led to a modest 2.5-fold increase in *CgCDR1* levels, whereas no up-regulation was observed for *CgSNQ2* and *CgPDR1* transcripts. Similarly, fluconazole- and staurosporine-treated cells failed to display a significant increase in the efflux of R6G in response to glucose (Fig. 8*D*), indicating that staurosporine-mediated inhibition of CgPkc1 signaling impedes the activation of multidrug efflux pumps upon fluconazole exposure.

## DISCUSSION

Invasive mycoses pose a serious therapeutic challenge, and resistance of fungal pathogens to current antifungal targets is a major clinical issue (2). A search for new fungal-specific drugs and a better understanding of the cellular stress survival processes of pathogenic fungi will help tackle this clinical challenge. In the current study, we have carried out a large unbiased screen for mutants that allow azoles to kill an intrinsically azole-resistant fungal pathogen *C. glabrata.* Using methylene blue to stain inviable cells, we distinguished *C. glabrata* mutants undergoing growth arrest from the mutants losing viability in the presence of fluconazole. This screen of 9134 random Tn7 insertional mutants identified a total of 7 genes required specifically for survival of *C. glabrata* during fluconazole stress (Table 1). These genes belong to one of the four biological processes: RNA polymerase II-mediated transcription, ergosterol biosynthesis, actin cytoskeleton organization, and Rho1-mediated signaling, suggesting that these processes play a crucial role in survival of azole stress in *C. glabrata.* Of the seven genes identified, only the *S. cerevisiae* ortholog of *CgSLT2* has previously been implicated in survival during antifungal stress. Furthermore, although the Gal11/Med15 subunit of the mediator co-activator complex has recently been reported to be essential for CgPdr1-regulated expression of multidrug efflux pumps in *C. glabrata* (14), we report for the first time that disruption of putative RNA polymerase II mediator complex subunits encoded by *CgMED2* and *CgPGD1* results in loss of viability during azole stress.

Our results suggest a pivotal role for Rho1-regulated CgPkc1 signaling in modulating gene expression and enabling survival in the presence of azole antifungals. Of seven mutants selected from the genome-wide screen, three had Tn7 insertions in the genes implicated in Rho GTPase-mediated signal transduction cascade (Table 1). These genes code for a negative regulator of CgRho1 GTPase (CgBem2), a serine/threonine MAPK (CgSlt2), and a formin protein (CgBnr1).

Blast analysis revealed the presence of seven small Rho GTPases and seven proteins containing RhoGAP domain in the *C. glabrata* genome (supplemental Table S3). The morphology defects and presence of higher amounts of active (GTP-bound) Rho GTPase and of phosphorylated CgSlt2 in mutants lacking *CgBEM2* suggest that CgBem2 functions as a GAP for CgRho1, consistent with its known role in *S. cerevisiae* (53). The Rho family of GTPases is known to perform myriad functions in diverse cellular processes through different effector molecules partly due to the target specificities, functional diversities, and individual regulation of their GAPs (26, 54). Notably, although disruption of CgBem2 led to constitutive activation of Rho1-regulated CgPkc1-mediated signaling, the unique budding, thermal, and morphogenetic defects of *Cgbem2* mutants suggest that downstream components of CgPkc1-mediated CWI pathway are not involved in actin organization and cell morphogenesis in *C. glabrata*. Thus, it is plausible that the seven GAPs in *C. glabrata* may selectively regulate the activities of multiple effector proteins of Rho family of small GTPases, thereby enabling GTPases to play a critical role in diverse physiological processes.

Bem2 in *S. cerevisiae* acts as a GAP for Rho1 and is implicated in antifungal sensitivity (assumed to be due to increased permeability of the cell surface), actin cytoskeleton organization, and bud emergence (35, 36). These functions of Bem2 seem to be conserved between *S. cerevisiae* and *C. glabrata*, as the mutants lacking Bem2 in *C. glabrata* displayed many biochemical and cell biological aspects that match the phenotypes in *S. cerevisiae*. However, our work has also uncovered novel and unexpected roles for *CgBEM2* in the survival of fluconazole stress and in the up-regulation of multidrug efflux pumps upon fluconazole exposure. Efflux pumps play a major role in azole susceptibility, and clinical resistance has been attributed to the up-regulation of drug transporters in *C. glabrata* (8, 11). Our data demonstrate that expression and activity of multidrug transporters in response to fluconazole is modulated by the disruption of CgBem2, a negative regulator of CgRho1. Mutants lacking CgBem2 have constitutively active CgPkc1-mediated CWI pathway and were able to both elevate the transcript and the protein levels as well as the phosphorylation of CgSlt2 upon fluconazole exposure. However, they were unable to activate the expression of multidrug transporters and lost viability in the presence of fluconazole. The precise mechanism linking *CgBEM2* function with efflux pump activation and survival of

azole stress remains to be determined, but the staurosporine-mediated partial rescue of fluconazole-induced viability loss in *Cgbem2*Δ cells implicates CgPkc1 signaling. Intriguingly, staurosporine-mediated inhibition of CgPkc1 signaling in wild-type cells phenocopies the effects of CgBem2 deletion, as staurosporine-treated wild-type cells were found to be compromised for their response to azole stress (Figs. 7*B* and 8, *C* and *D*). The findings that both the constitutive activation (*Cgbem2*Δ) and the inhibition of CgPkc1-mediated signaling (staurosporine treatment) result in viability loss during azole stress suggest that PKC signaling is tightly regulated in *C. glabrata* and any aberration results in an inability to mount a proper cellular stress response leading to cell death. Identification of the effector protein(s) of CgBem2 responsible for the modulation of *CDR* gene expression in response to azole stress in *C. glabrata* will be the focus of future investigations.

Intriguingly, ploidy-dependent gene regulation plays an important role in drug susceptibility, and resistance to fluconazole in *C. albicans* has been associated with increased copy number of azole resistance genes due to acquired aneuploidy (55). However, the enhanced susceptibility of *Cgbem2*Δ cells toward fluconazole, despite their polyploidy nature, probably indicates impaired ability to maintain genomic stability due to defective morphogenesis.

We have previously shown that fluconazole in conjunction with FK506 is fungicidal in *C. glabrata* (10). In the present study, we show that despite the lack of intrinsic antifungal activity, staurosporine- and geldanamycin-mediated inhibition of CgPkc1 and CgHsp90, respectively, led to survival defects for wild-type cells in the presence of fluconazole, implying that multiple signaling cascades operate to ensure cell survival during azole stress in *C. glabrata*. These findings are in accord with the results obtained by other groups linking PKC signaling to tolerance of antifungals in *S. cerevisiae* and *C. albicans* (18, 22, 50) and suggest a broad conservation of cellular mechanisms to survive antifungal drug stress in fungal species. In conclusion, we report for the first time that CgBem2, a negative regulator of CgRho1 GTPase, is essential for survival of azole stress and for the up-regulation of genes coding for multidrug transporters upon fluconazole exposure.

*Acknowledgments—We acknowledge the help of Munmun Chatterjee and K. G. Rajaneesh in creating plasmids and strains for disruption of CgBEM2 and CgPAN1. We thank Brian Green and Shih-Jung Pan for sharing reagents and protocols to generate C. glabrata knock-out strains by fusion-PCR methodology. We are grateful to Brendan Cormack, Anand Bachhawat, Rashna Bhandari, and Subhadeep Chatterjee for critical reading of the manuscript and useful comments.*

## REFERENCES


1. Messer, S. A., Jones, R. N., and Fritsche, T. R. (2006) *J. Clin. Microbiol.* **44,** 1782–1787
2. Pfaller, M. A., and Diekema, D. J. (2007) *Clin. Microbiol. Rev.* **20,** 133–163
3. Pfaller, M. A., Diekema, D. J., Gibbs, D. L., Newell, V. A., Ellis, D., Tullio, V., Rodloff, A., Fu, W., and Ling, T. A. (2010) *J. Clin. Microbiol.* **48,** 1366–1377
4. Hazen, K. C., Baron, E. J., Colombo, A. L., Girmenia, C., Sanchez-Sousa, A., del Palacio, A., de Bedout, C., and Gibbs, D. L. (2003) *J. Clin. Microbiol.* **41,** 5623–5632
5. Grant, S. M., and Clissold, S. P. (1990) *Drugs* **39,** 877–916
6. Akins, R. A. (2005) *Med. Mycol.* **43,** 285–318
7. Geber, A., Hitchcock, C. A., Swartz, J. E., Pullen, F. S., Marsden, K. E., Kwon-Chung, K. J., and Bennett, J. E. (1995) *Antimicrob. Agents Chemother.* **39,** 2708–2717
8. Sanglard, D., Ischer, F., Calabrese, D., Majcherczyk, P. A., and Bille, J. (1999) *Antimicrob. Agents Chemother.* **43,** 2753–2765
9. Izumikawa, K., Kakeya, H., Tsai, H. F., Grimberg, B., and Bennett, J. E. (2003) *Yeast* **20,** 249–261
10. Kaur, R., Castaño, I., and Cormack, B. P. (2004) *Antimicrob. Agents Chemother.* **48,** 1600–1613
11. Torelli, R., Posteraro, B., Ferrari, S., La Sorda, M., Fadda, G., Sanglard, D., and Sanguinetti, M. (2008) *Mol. Microbiol.* **68,** 186–201
12. Tsai, H. F., Krol, A. A., Sarti, K. E., and Bennett, J. E. (2006) *Antimicrob. Agents Chemother.* **50,** 1384–1392
13. Vermitsky, J. P., Earhart, K. D., Smith, W. L., Homayouni, R., Edlind, T. D., and Rogers, P. D. (2006) *Mol. Microbiol.* **61,** 704–722
14. Thakur, J. K., Arthanari, H., Yang, F., Pan, S. J., Fan, X., Breger, J., Frueh, D. P., Gulshan, K., Li, D. K., Mylonakis, E., Struhl, K., Moye-Rowley, W. S., Cormack, B. P., Wagner, G., and Näär, A. M. (2008) *Nature* **452,** 604–609
15. Berila, N., Borecka, S., Dzugasova, V., Bojnansky, J., and Subik, J. (2009) *Int. J. Antimicrob. Agents* **33,** 574–578
16. Kaur, R., Domergue, R., Zupancic, M., and Cormack, B. P. (2005) *Curr. Opin. Microbiol.* **8,** 378–384
17. Bahn, Y. S., Xue, C., Idnurm, A., Rutherford, J. C., Heitman, J., and Cardenas, M. E. (2007) *Nat. Rev. Microbiol.* **5,** 57–69
18. Bonilla, M., Nastase, K. K., and Cunningham, K. W. (2002) *EMBO J.* **21,** 2343–2353
19. Onyewu, C., Blankenship, J. R., Del Poeta, M., and Heitman, J. (2003) *Antimicrob. Agents Chemother.* **47,** 956–964
20. Jain, P., Akula, I., and Edlind, T. (2003) *Antimicrob. Agents Chemother.* **47,** 3195–3201
21. Cowen, L. E., and Lindquist, S. (2005) *Science* **309,** 2185–2189
22. LaFayette, S. L., Collins, C., Zaas, A. K., Schell, W. A., Betancourt-Quiroz, M., Gunatilaka, A. A., Perfect, J. R., and Cowen, L. E. (2010) *PLoS Pathog.* **6,** e1001069
23. Levin, D. E. (2005) *Microbiol. Mol. Biol. Rev.* **69,** 262–291
24. Martín, H., Rodríguez-Pachón, J. M., Ruiz, C., Nombela, C., and Molina, M. (2000) *J. Biol. Chem.* **275,** 1511–1519
25. Nonaka, H., Tanaka, K., Hirano, H., Fujiwara, T., Kohno, H., Umikawa, M., Mino, A., and Takai, Y. (1995) *EMBO J.* **14,** 5931–5938
26. Perez, P., and Rincón, S. A. (2010) *Biochem. J.* **426,** 243–253
27. Gray, J. V., Ogas, J. P., Kamada, Y., Stone, M., Levin, D. E., and Herskowitz, I. (1997) *EMBO J.* **16,** 4924–4937
28. Heinisch, J. J., Lorberg, A., Schmitz, H. P., and Jacoby, J. J. (1999) *Mol. Microbiol.* **32,** 671–680
29. Castano, I., Kaur, R., Pan, S., Cregg, R., Penas, Ade, L., Guo, N., Biery, M. C., Craig, N. L., and Cormack, B. P. (2003) *Genome Res.* **13,** 905–915
30. Sabatinos, S. A., and Forsburg, S. L. (2009) *Methods Mol. Biol.* **521,** 449–461
31. Emter, R., Heese-Peck, A., and Kralli, A. (2002) *FEBS Lett.* **521,** 57–61
32. Bairwa, G., and Kaur, R. (2011) *Mol. Microbiol.* **79,** 900–913
33. van den Hazel, H. B., Pichler, H., do Valle Matta, M. A., Leitner, E., Goffeau, A., and Daum, G. (1999) *J. Biol. Chem.* **274,** 1934–1941
34. Painting, K., and Kirsop, B. (1990) *World J. Microbiol. Biotechnol.* **6,** 346–347
35. Cid, V. J., Cenamor, R., Sánchez, M., and Nombela, C. (1998) *Microbiology* **144,** 25–36
36. Wang, T., and Bretscher, A. (1995) *Mol. Biol. Cell* **6,** 1011–1024
37. Wendland, B., and Emr, S. D. (1998) *J. Cell Biol.* **141,** 71–84
38. Myers, L. C., Gustafsson, C. M., Bushnell, D. A., Lui, M., Erdjument-Bromage, H., Tempst, P., and Kornberg, R. D. (1998) *Genes Dev.* **12,** 45–54
39. Myers, L. C., Gustafsson, C. M., Hayashibara, K. C., Brown, P. O., and Kornberg, R. D. (1999) *Proc. Natl. Acad. Sci. U.S.A.* **96,** 67–72
40. de Nobel, H., Ruiz, C., Martin, H., Morris, W., Brul, S., Molina, M., and Klis, F. M. (2000) *Microbiology* **146,** 2121–2132
41. Imamura, H., Tanaka, K., Hihara, T., Umikawa, M., Kamei, T., Takahashi, K., Sasaki, T., and Takai, Y. (1997) *EMBO J.* **16,** 2745–2755

42. Caudle, K. E., Barker, K. S., Wiederhold, N. P., Xu, L., Homayouni, R., and Rogers, P. D. (2011) *Eukaryot. Cell* **10,** 373–383
43. Madden, K., Sheu, Y. J., Baetz, K., Andrews, B., and Snyder, M. (1997) *Science* **275,** 1781–1784
44. Dujon, B., Sherman, D., Fischer, G., Durrens, P., Casaregola, S., Lafontaine, I., De Montigny, J., Marck, C., Neuvéglise, C., Talla, E., Goffard, N., Frangeul, L., Aigle, M., Anthouard, V., Babour, A., Barbe, V., Barnay, S., Blanchin, S., Beckerich, J. M., Beyne, E., Bleykasten, C., Boisramé, A., Boyer, J., Cattolico, L., Confanioleri, F., De Daruvar, A., Despons, L., Fabre, E., Fairhead, C., Ferry-Dumazet, H., Groppi, A., Hantraye, F., Hennequin, C., Jauniaux, N., Joyet, P., Kachouri, R., Kerrest, A., Koszul, R., Lemaire, M., Lesur, I., Ma, L., Muller, H., Nicaud, J. M., Nikolski, M., Oztas, S., Ozier-Kalogeropoulos, O., Pellenz, S., Potier, S., Richard, G. F., Straub, M. L., Suleau, A., Swennen, D., Tekaia, F., Wésolowski-Louvel, M., Westhof, E., Wirth, B., Zeniou-Meyer, M., Zivanovic, I., Bolotin-Fukuhara, M., Thierry, A., Bouchier, C., Caudron, B., Scarpelli, C., Gaillardin, C., Weissenbach, J., Wincker, P., and Souciet, J. L.) (2004) *Nature* **430,** 35–44
45. Kohno, H., Tanaka, K., Mino, A., Umikawa, M., Imamura, H., Fujiwara, T., Fujita, Y., Hotta, K., Qadota, H., Watanabe, T., Ohya, Y., and Takai, Y. (1996) *EMBO J.* **15,** 6060–6068
46. Miyazaki, T., Inamine, T., Yamauchi, S., Nagayoshi, Y., Saijo, T., Izumikawa, K., Seki, M., Kakeya, H., Yamamoto, Y., Yanagihara, K., Miyazaki, Y., and Kohno, S. (2010) *FEMS Yeast Res.* **10,** 343–352
47. Sachs, A. B., and Deardorff, J. A. (1992) *Cell* **70,** 961–973
48. Marquitz, A. R., Harrison, J. C., Bose, I., Zyla, T. R., McMillan, J. N., and Lew, D. J. (2002) *EMBO J.* **21,** 4012–4025
49. Baetz, K., Moffat, J., Haynes, J., Chang, M., and Andrews, B. (2001) *Mol. Cell. Biol.* **21,** 6515–6528
50. Bonilla, M., and Cunningham, K. W. (2003) *Mol. Biol. Cell* **14,** 4296–4305
51. Cota, J. M., Grabinski, J. L., Talbert, R. L., Burgess, D. S., Rogers, P. D., Edlind, T. D., and Wiederhold, N. P. (2008) *Antimicrob. Agents Chemother.* **52,** 1144–1146
52. Wada, S., Tanabe, K., Yamazaki, A., Niimi, M., Uehara, Y., Niimi, K., Lamping, E., Cannon, R. D., and Monk, B. C. (2005) *J. Biol. Chem.* **280,** 94–103
53. Peterson, J., Zheng, Y., Bender, L., Myers, A., Cerione, R., and Bender, A. (1994) *J. Cell Biol.* **127,** 1395–1406
54. Bernards, A. (2003) *Biochim. Biophys. Acta* **1603,** 47–82
55. Selmecki, A. M., Dulmage, K., Cowen, L. E., Anderson, J. B., and Berman, J. (2009) *PLoS Genet.* **5,** e1000705

Microbiology:


# The Rho1 GTPase-activating Protein CgBem2 Is Required for Survival of Azole Stress in *Candida glabrata*

Sapan Borah, Raju Shivarathri and Rupinder Kaur

*J. Biol. Chem. 2011, 286:34311-34324.*
*doi: 10.1074/jbc.M111.264671 originally published online August 8, 2011*